Effect of high oxygen pressure annealing on superconducting $Nd_{1.85}Ce_{0.15}CuO_4$ thin films by pulsed laser deposition from Cu-enriched targets

M Hoek, F Coneri, D P Leusink, P D Eerkes, X Renshaw Wang and H Hilgenkamp[†]

Faculty of Science and Technology and MESA+ Institute for Nanotechnology, University of Twente, 7500 AE Enschede, The Netherlands

E-mail: m.hoek@utwente.nl

Abstract. We show that the quality of $Nd_{1.85}Ce_{0.15}CuO_4$ films grown by pulsed laser deposition can be enhanced by using a non-stoichiometric target with extra copper added to suppress the formation of a parasitic $(Nd,Ce)_2O_3$ phase. The properties of these films are less dependent on the exact annealing procedure after deposition as compared to films grown from a stoichiometric target. Film growth can be followed by a 1 bar oxygen annealing, after an initial vacuum annealing, while retaining the superconducting properties and quality. This enables the integration of electron-doped cuprates with their hole-doped counterparts on a single chip, to create, for example, superconducting *pn*-junctions.

PACS numbers: 74.72.-h, 74.62.Bf, 74.72.Ek, 74.25.F, 74.78.-w, 74.78.Fk

† also at: Institute-Lorentz, Leiden University, 2300 RA Leiden, The Netherlands

1. Introduction

With the substitutional doping in cuprates by Ce in electron-doped $Nd_{2-x}Ce_xCuO_4$ and Sr in hole-doped $La_{2-x}Sr_xCuO_4$, the parallel to semiconductors is easy to make. Indeed, various theoretical analyses have been made on the properties and possibilities of combinations of electron- and hole-doped cuprates, ranging from the formation of a Mott insulator depletion zone [1], unconventional Josephson junctions [2, 3] and superradiant light emission [4]. Oxygen plays an important role in the realization of combinations of electron- and hole-doped cuprates. The role of oxygen in n-type cuprates is widely researched and debated [5, 7, 6, 8, 9, 10, 11, 12]. The consensus is that an oxygen reduction is necessary for superconductivity and that strong oxygenation leads to loss of superconductivity and increasing resistance. However, the exact mechanism for oxygen reduction is still under debate, in particular where oxygen is removed from the unit cell and what the consequences are for the structure of the cuprate [9, 10, 11, 13]. The necessity of a reduction is in stark contrast with the oxygenation needed for optimal superconductivity in the p-type cuprates: in general, p-type cuprates require an oxygenation step at high oxygen pressures. These conflicting annealing requirements are one of the main hurdles to realize combinations of electron- and hole-doped cuprates.

   In this work we investigate the effect of strong oxygenation, needed for the growth of a p-type cuprate like $La_{2-x}Sr_xCuO_4$, on the n-type cuprate $Nd_{2-x}Ce_xCuO_4$. Growth of $RE_{2-x}Ce_xCuO_4$ (RE = Nd, Pr, ...) as single crystals grown by e.g. the traveling-solvent floating-zone technique [11, 14, 15, 16] or as thin films by pulsed laser deposition (PLD) [12, 13, 17, 18] is almost always accompanied by the formation of a parasitic phase of $(RE,Ce)_2O_3$, due to copper deficiency during growth and during oxygen reduction. Other techniques like molecular beam epitaxy [19] and dc sputtering [20] appear to be less sensitive to the formation of the $(RE,Ce)_2O_3$ phase. For PLD, it has been shown that this parasitic phase can be suppressed in $Pr_{2-x}Ce_xCuO_4$ by adding extra copper to the PLD target [13]. We show that the parasitic $(Nd,Ce)_2O_3$ phase in $Nd_{1.85}Ce_{0.15}CuO_4$ can also be suppressed by using copper-rich targets and that these films retain their quality and superconducting properties when subjected to oxygen annealing procedures suitable for the growth of p-type cuprates.

2. Experimental details

We compare films grown by PLD using two different targets with effective compositions $Nd_{1.85}Ce_{0.15}CuO_4$ (NCCO) and $Nd_{1.85}Ce_{0.15}Cu_{1.1}O_4$ (NCCO+), the latter containing 10% extra copper. The targets are prepared by solid state synthesis and the crystal structure is verified by X-ray powder diffraction. The films are deposited at a heater temperature of 820 °C in 0.25 mbar oxygen using a KrF excimer laser with a fluency of 1.2 J/cm^2, a spot size of 5.7 mm^2 and a repetition rate of 4 Hz. All films are grown on (001) oriented $[LaAlO_3]_{0.3}[Sr_2AlTaO_6]_{0.7}$ (LSAT) substrates that have been annealed in flowing oxygen for 10 hours at 1050 °C to obtain an atomically smooth surface, as

measured by atomic force microscopy (AFM). We have grown films varying in thickness between 30 and 500 nm, with most of the films being 70 nm. We have chosen this value with future device fabrication requirements in mind, although with this thickness the lattice strain from the substrate slightly suppresses T_c [18].

We have investigated three different annealing procedures for the $Nd_{1.85}Ce_{0.15}CuO_4$ films. The first is a standard vacuum annealing where the film is cooled down from 820 °C in deposition pressure and then annealed in vacuum for 8 minutes at 740 °C followed by a cool down in vacuum at 10 °C/min. The other two procedures are two opposite cases, to explore the stability of the $Nd_{1.85}Ce_{0.15}CuO_4$ films under long reduction and strong oxygenation, respectively. For the long reduction, the dwell time at 740 °C is extended to 45 minutes. For the strong oxygenation procedure there is an initial 8 minute vacuum annealing at 740 °C and then at 600 °C the conditions are changed to a common recipe we employ for p-doped superconductors like $La_{2-x}Sr_xCuO_4$ and $YBa_2Cu_3O_{7-\delta}$. Here, the film is first annealed in 1 bar oxygen for 15 minutes at 600 °C and then for 30 minutes at 450 °C and subsequently cooled down further in 1 bar oxygen.

The film thickness and quality is investigated by X-ray diffraction (XRD), cross-sectional transmission electron microscopy (TEM) and by AFM. The thickness is measured by AFM using an edge fabricated by a hard mask lift-off of amorphous $YBa_2Cu_3O_{7-\delta}$ (lift-off using 1% H_3PO_4) or gold (lift-off using a KI solution). XRD shows that all films are c-axis oriented with a c-axis length of 12.08(1) Å, this is also what is observed for optimally doped single crystal [16]. We measure an RMS surface rougness with AFM on a scan area of 2 μm × 2 μm of 3 nm for the $Nd_{1.85}Ce_{0.15}CuO_4$ films grown using the target with extra copper and 1.5 nm for the $Nd_{1.85}Ce_{0.15}CuO_4$ films from the stoichiometric target, both for films of 70 nm thickness.

The samples are contacted at the corners by Al bond wires on Au/Ti contact pads in a standard Van der Pauw geometry for sheet resistance and Hall measurements in a Quantum Design 9 T PPMS system. Hall measurements are performed up to 4 T and for low temperatures up to 9 T. The sheet resistance is measured both during warm up and cool down at a rate varying between 0.1 °C and 3 °C per minute.

3. Results and discussion

3.1. Suppression of the (Nd,Ce)₂O₃ parasitic phase

This section compares films grown using the targets with and without extra copper added. Figures 1, 2 and 3 compare the same two samples, representative for the general behavior we have observed, both are 70 nm thick and are annealed in vacuum for 8 minutes at 740 °C after deposition. Figure 1 shows a detail of the XRD $\theta - 2\theta$ spectra for the two $Nd_{1.85}Ce_{0.15}CuO_4$ films, grown with and without extra copper in the target, showing the $Nd_{1.85}Ce_{0.15}CuO_4$ (004) and the (Nd,Ce)₂O₃ (004) reflection. Both films have been annealed for 8 minutes in vacuum at 740 °C. The spectra are
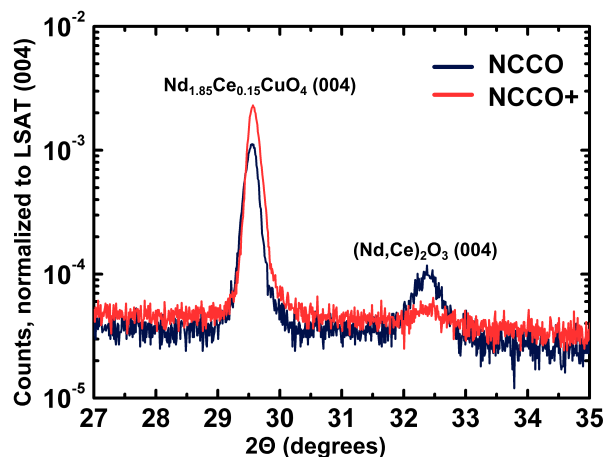
Figure 1. Detail of X-ray diffraction $\theta - 2\theta$ scans normalized to the LSAT(004) peak (not shown in figure) on 70 nm $Nd_{1.85}Ce_{0.15}CuO_4$ films deposited from the stoichiometric target (NCCO, blue) and the non-stoichiometric target with extra copper added (NCCO+, red), showing the suppression of the parasitic $(Nd,Ce)_2O_3$ phase. Both samples have been annealed for 8 minutes in vacuum at 740 °C.

normalized to the (002) Bragg reflection of LSAT (not shown in the figure). With the addition of extra copper to the target, we see a reduction of nearly an order of magnitude in the ratio between the intensities of the $(Nd,Ce)_2O_3$ (004) diffraction peak and the $Nd_{1.85}Ce_{0.15}CuO_4$ (004) peak. Together with this reduction, we observe a higher intensity for the $Nd_{1.85}Ce_{0.15}CuO_4$ (004) peak, while the full width at half maximum is slightly decreased (from 0.23° to 0.19°), indicating a higher crystallinity for the films grown with extra copper. The $(Nd,Ce)_2O_3$ phase is still not fully suppressed, suggesting that an even higher percentage of copper may be required for full suppression. We find no appreciable difference in the c-axis lattice parameter between the different annealing procedures for films grown with either of the two targets.

Figure 2 shows TEM close ups of two $Nd_{1.85}Ce_{0.15}CuO_4$ films near the substrate/film interface, grown using the two targets without, figure 2(a), and with extra copper, figure 2(b), both annealed in vacuum for 8 minutes at 740 °C. For the film grown using the stoichiometric target, the presence of the parasitic $(Nd,Ce)_2O_3$ phase is inferred from the appearance of Moiré patterns in the TEM image. The image shows the crystal planes of $Nd_{1.85}Ce_{0.15}CuO_4$ and areas with a different periodicity; here, a Moiré pattern is formed by an overlap of the $Nd_{1.85}Ce_{0.15}CuO_4$ lattice with the lattice of the $(Nd,Ce)_2O_3$ parasitic phase, namely the $Nd_{1.85}Ce_{0.15}CuO_4$ (103) lattice planes and the $(Nd,Ce)_2O_3$ (222) lattice planes. The (103) and the (222) planes are sketched in figure 2(a), as well as a set of overlapping planes on top of one of the Moiré patterns. The planes are not arbitrary, $Nd_{1.85}Ce_{0.15}CuO_4$ (103) and $(Nd,Ce)_2O_3$ (222) are also the planes that would give the strongest signal in X-ray powder diffraction. The periodicity of the Moiré pattern (d_M) can be calculated from the difference between the g-vectors of the
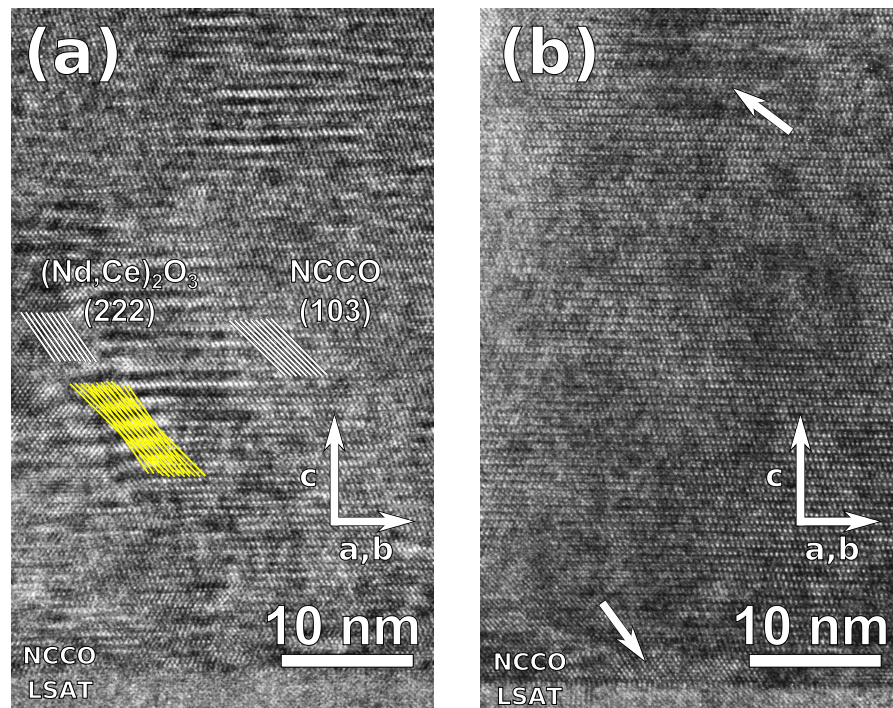
Effect of high oxygen pressure annealing on superconducting $Nd_{1.85}Ce_{0.15}CuO_4$ ...   5

Figure 2. Transmission electron microscopy close ups near the substrate of 70 nm $Nd_{1.85}Ce_{0.15}CuO_4$ films deposited from the stoichiometric target (a) and the non-stoichiometric target with extra copper added (b), both annealed for 8 minutes in vacuum at 740 °C after deposition. (a) $Nd_{1.85}Ce_{0.15}CuO_4$ from the stoichiometric target shows Moiré fringes (indicated by the yellow lines), caused by the overlapping of the $Nd_{1.85}Ce_{0.15}CuO_4$ (103) lattice planes and the $(Nd,Ce)_2O_3$ (222) lattice planes, both identified by the white lines; (b) $Nd_{1.85}Ce_{0.15}CuO_4$ from the non-stoichiometric target with extra copper shows higher $Nd_{1.85}Ce_{0.15}CuO_4$ phase purity with only a small inclusion of the parasitic phase, indicated by the white arrows in the top and the bottom of the figure.

individual lattices [21]:

$$d_M = \frac{d_{(103)}d_{(222)}}{\sqrt{d_{(103)}^2 + d_{(222)}^2 - 2d_{(103)}d_{(222)}\cos\beta}}, \tag{1}$$

where $d_{(103)}$ and $d_{(222)}$ are the lattice spacing of the $Nd_{1.85}Ce_{0.15}CuO_4$ (103) planes and the $(Nd,Ce)_2O_3$ (222) planes, respectively, and β is the angle in radians between the g-vectors, normal to these planes. Using the lattice parameters for $Nd_{1.85}Ce_{0.15}CuO_4$ and $(Nd,Ce)_2O_3$ from Kimura *et al.* [16] ($d_{(103)} = 2.82$ Å, $d_{(222)} = 3.22$ Å and $\beta = 0.16$ rad), we find an expected Moiré pattern spacing of 14.4 Å, which is also what we observe in the TEM images.

With the addition of extra copper to the target, we observe a significantly lower density of the parasitic phase in the film. Figure 2(b) is a typical example, showing a higher $Nd_{1.85}Ce_{0.15}CuO_4$ phase purity with only a small inclusion of the parasitic phase at the substrate interface and in the top of the image (indicated with white arrows). As was also observed in XRD, see figure 1, the parasitic phase is strongly, but not

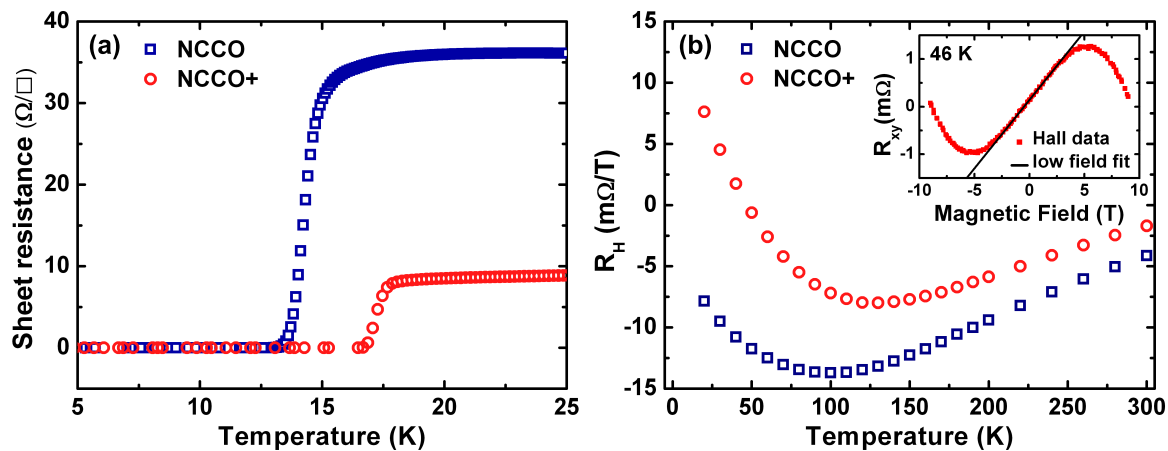*Effect of high oxygen pressure annealing on superconducting* $Nd_{1.85}Ce_{0.15}CuO_4$ ... 6

completely, suppressed.

Figure 3. Transport measurements on 70 nm $Nd_{1.85}Ce_{0.15}CuO_4$ films deposited from the stoichiometric target (NCCO, blue squares) and the non-stoichiometric target with extra copper added (NCCO+, red circles), both films are annealed in vacuum for 8 minutes at 740 °C. (a) Sheet resistance around T_c, showing a higher T_c, sharper transition and lower resistance for the $Nd_{1.85}Ce_{0.15}CuO_4$ film with extra copper; (b) Hall coefficient versus temperature measured in the Van der Pauw geometry, both films show a pronounced minimum and the $Nd_{1.85}Ce_{0.15}CuO_4$ grown from the target with extra copper shows a crossover to a positive Hall coefficient for low temperature. The inset shows the two-band nature of the Hall resistance at 46 K and a low field linear fit.

Figure 3 compares transport properties of the $Nd_{1.85}Ce_{0.15}CuO_4$ films. The suppression of the parasitic $(Nd,Ce)_2O_3$ phase is accompanied by in an increase of T_c by 3.5 K to a value of 16.7 K (T_{c0}) for films grown using the non-stoichiometric target, see figure 3(a). These films also show a sharper transition to the superconducting phase and a lower normal-state resistance. The sharper transition can be explained by a more homogeneous crystal structure for the films grown from the target with extra copper. The higher resistance for the $Nd_{1.85}Ce_{0.15}CuO_4$ films grown from the stoichiometric target may be explained by the $(Nd,Ce)_2O_3$ phase deforming nearby CuO_2 planes and acting as nucleation site for defects and dislocations, all increasing scattering.

The Hall coefficient for both films shows a trend generally observed for n-type cuprates around optimal doping, with an upturn towards positive values with decreasing temperature, indicating contribution of hole-like carriers [12, 22, 23, 24], see figure 3(b). For $Nd_{1.85}Ce_{0.15}CuO_4$ films grown from the target with extra copper, the minimum in the Hall coefficient shifts to a higher temperature. For low temperatures, a complete cross-over to a positive Hall coefficient is observed with a cross-over region where the Hall resistance displays both electron- and hole-like character, as shown in the inset to figure 3(b). The data in figure 3(b) only uses a low field linear fit to the Hall data, illustrated by the black linear fit in the inset. The difference between the two curves can be explained by the two band nature of $Nd_{2-x}Ce_xCuO_4$ around optimal doping. Here the Hall coefficient not only measures the carrier density, but a combination of

the density and mobility of both carrier types. As we argue that the suppression of the $(Nd,Ce)_2O_3$ phase decreases scattering, this will lead to a higher mobility, which will in turn be reflected in the Hall coefficient.
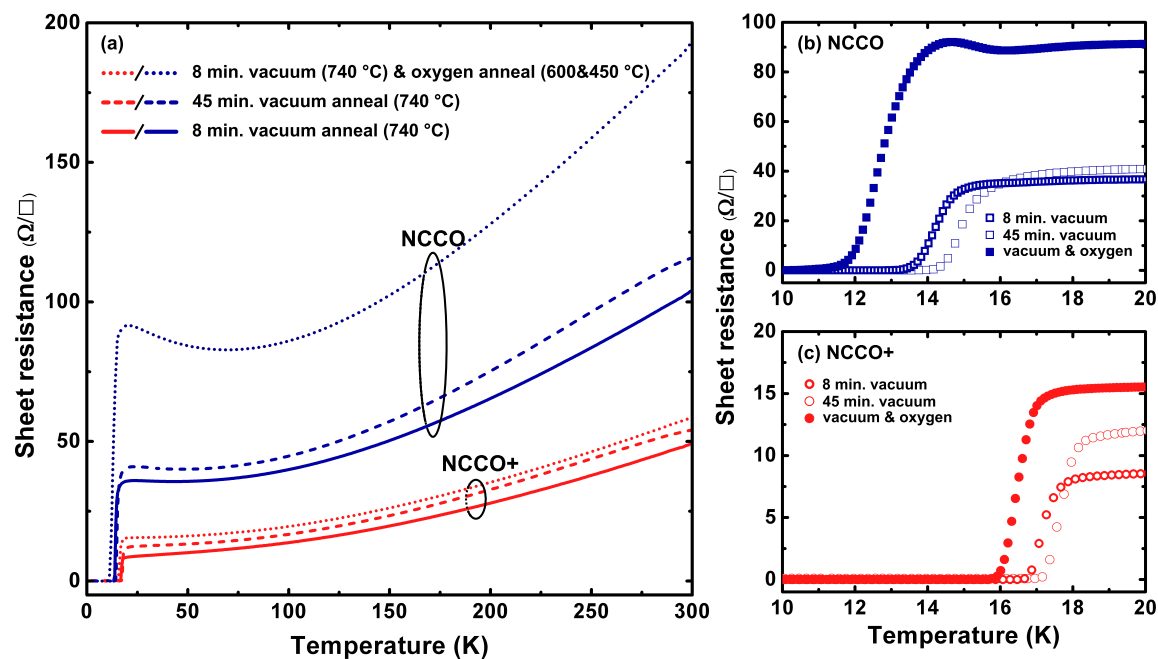

Figure 4. (a) Transport measurements on 70 nm $Nd_{1.85}Ce_{0.15}CuO_4$ films deposited from the stoichiometric target (NCCO, blue) and the non-stoichiometric target with extra copper added (NCCO+, red) for different annealing procedures: 8 minute vacuum annealing at 740 °C (solid lines), 45 minute vacuum annealing at 740 °C (dashed lines) and 8 minute vacuum annealing at 740 °C followed by a 1 bar oxygen annealing at 600 °C (15 min.) and 450 °C (30 min.) (dotted lines); (b) closeup around T_c for the $Nd_{1.85}Ce_{0.15}CuO_4$ films from the stoichiometric target; (c) closeup around T_c for the $Nd_{1.85}Ce_{0.15}CuO_4$ films with extra copper added to the target.

3.2. Effect of different annealing procedures

Finally, we look at the effect of different annealing procedures for films grown using the stoichiometric target and the target with extra copper added. The three annealing procedures are as described earlier: 8 minutes vacuum, 45 minutes vacuum, and 8 minutes vacuum followed by 1 bar oxygen at 600 °C (15 min.) and 450 °C (30 min.). The sheet resistance for all films across the whole temperature range (2-300 K) is shown in figure 4(a). The films grown from the target with extra copper show a close grouping of the curves, whereas the films grown with the stoichiometric target show a large spread. The largest deviation is found for the $Nd_{1.85}Ce_{0.15}CuO_4$ films grown using the stoichiometric target and annealed in oxygen after the vacuum annealing. Here, an upturn in the resistance is observed above T_c, indicating a shift to lower doping by oxygen inclusion [9], increased impurity scattering and carrier localization [23, 25]. At T_c, these samples show a broad transition with a small upturn at T_c, characteristic

Effect of high oxygen pressure annealing on superconducting $Nd_{1.85}Ce_{0.15}CuO_4$ ...   8

for sheet measurements on inhomogeneous superconductors with an out-of-line contact arrangement [26], see figure 4(b). We find the highest T_c for films annealed for 45 minutes in vacuum.

The films grown with the target with extra copper show only a 2 K spread in T_c with the different annealing procedures and the width of the superconducting transition is always smaller than 1 K. The same trend as for the films without extra copper is observed, with a 45 minute vacuum annealing giving the highest T_c and a 1 bar oxygen annealing at 600 °C the lowest T_c, see figure 4(c). All films with extra copper show a higher T_c than the films grown with the stoichiometric target.
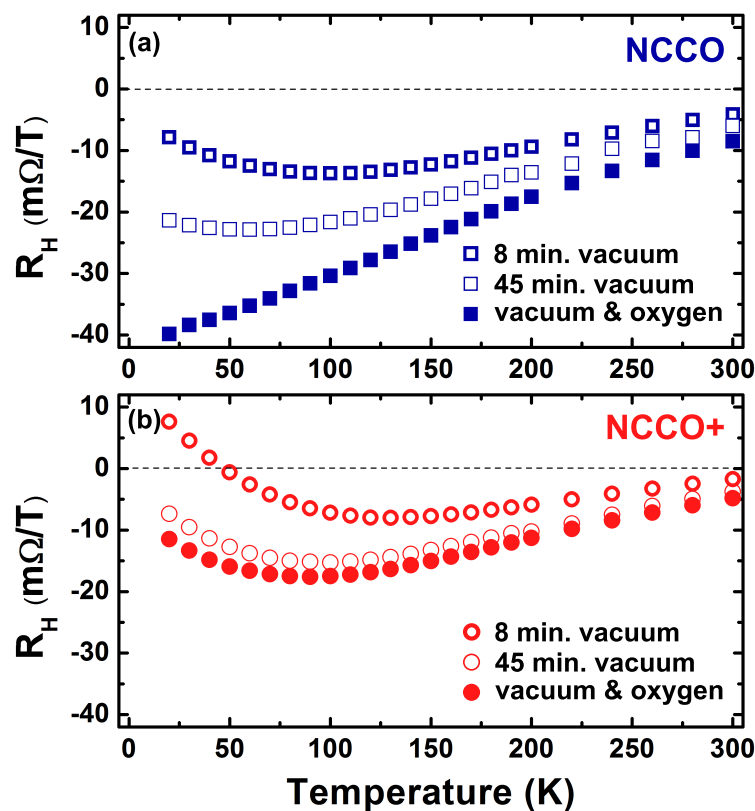

Figure 5. Hall measurements on 70 nm $Nd_{1.85}Ce_{0.15}CuO_4$ films deposited from the stoichiometric target (a) and the non-stoichiometric target with extra copper added (b) for different annealing procedures: 8 minute vacuum annealing at 740 °C (half filled symbols), 45 minute vacuum annealing at 740 °C (open symbols) and 8 minute vacuum annealing at 740 °C followed by a 1 bar oxygen annealing at 600 °C (15 min.) and 450 °C (30 min.) (closed symbols).

The Hall effect measurements confirm the observations from the sheet resistance measurements, see figure 5(a,b). The $Nd_{1.85}Ce_{0.15}CuO_4$ films grown with the standard target show a wide spread in the Hall coefficient, especially at low temperatures, where

the characteristic minimum has completely disappeared for the films annealed in oxygen, see figure 5(a). This was also reported for oxygenated films of $Nd_{2-x}Ce_xCuO_4$ [23] and $Pr_{2-x}Ce_xCuO_4$ [10]. For the $Nd_{1.85}Ce_{0.15}CuO_4$ films with extra copper we see a closer grouping of all the curves and they all show the characteristic minimum, see figure 5(b). It is interesting to note that both a longer vacuum annealing and an oxygen annealing following a short vacuum annealing suppresses the cross-over to a positive Hall coefficient, not depending on the presence of the parasitic $(Nd,Ce)_2O_3$ phase. In the latter case this can be explained by the counter-doping effect of oxygen, effectively shifting the doping away from optimal doping, towards underdoping [9]. The former case is not immediately obvious. The cross-over to positive Hall coefficients for the extra copper films with an 8 minute vacuum annealing, suggests that the samples are already at optimal doping or even overdoped. It has been shown that, during vacuum annealing, oxygen is removed from the CuO_2 planes, suppressing anti-ferromagnetic ordering and promoting hole-like carriers [6, 8, 10, 27]. This is accompanied by an increased normal-state resistance for over-reduction [23, 28, 29], attributed to increased defect and impurity scattering [27]. Annealing for 45 minutes should therefore only shift the Hall coefficient towards more hole-like character, as is commonly observed for oxygen reduction in $Nd_{2-x}Ce_xCuO_4$ [23, 25, 30]. This is not what we observe, we do see an increased normal-state resistance, but the Hall coefficients shifts toward more negative values. We suggest that as more and more oxygen is removed from the CuO_2 planes, scattering is increased. As the Hall coefficient for a two-band system is also linked to the mobility of the carriers, our observations can be explained by the scattering centers having more influence on the mobility of the hole-like carriers than on the electron-like carriers. This would explain both the higher normal state resistivity and the shift to a more negative Hall coefficient.

4. Conclusions

Our experiments show that the addition of extra copper to the PLD target of $Nd_{1.85}Ce_{0.15}CuO_4$ can increase the quality and T_c of thin films by suppressing the formation of the parasitic $(Nd,Ce)_2O_3$ phase. The presence or absence of the parasitic $(Nd,Ce)_2O_3$ phase in $Nd_{1.85}Ce_{0.15}CuO_4$ films has a strong influence on T_c and the transport properties above T_c. For long reduction the difference is minimal, while the biggest difference is observed for strong oxygenation. The relative minor influence of the exact annealing procedure on T_c and the Hall coefficient for $Nd_{1.85}Ce_{0.15}CuO_4$ films grown with extra copper in the target suggests that studies into the exact role of oxygen in the reduction process for n-type cuprates should not overlook the influence the presence of the $(RE,Ce)_2O_3$ parasitic phase can have. We have also shown that the $Nd_{1.85}Ce_{0.15}CuO_4$ films with extra copper can even be subjected to a 1 bar oxygen annealing suitable for the growth of p-type cuprates such as $La_{2-x}Sr_xCuO_4$ and $YBa_2Cu_3O_{7-\delta}$. This makes $Nd_{2-x}Ce_xCuO_4$ grown from a non-stoichiometric target with extra copper a prime candidate for studying pn-physics in the cuprate superconductors,

Effect of high oxygen pressure annealing on superconducting $Nd_{1.85}Ce_{0.15}CuO_4$ ...   10

opening the way to integrate electron-doped cuprates with their hole-doped counterparts on a single chip. Such combinations are of interest for example for the creation of superconducting *pn*-junctions or to explore electron-hole interactions in the rich phase diagram of the cuprates.

Acknowledgments

References

[1] Charlebois M, Hassan S R, Karan R, Sénéchal D and Tremblay A-M S 2012 *Phys. Rev. B* **87** 035137

[2] Mannhart J, Kleinsasser A, Ströbel J and Baratoff A 1993 *Physica C* **216** 401–16

[3] Hu J, Wu C and Dai X 2007 *Phys. Rev. Lett.* **99** 067004

[4] Hanamura E 2002 *Phys. Stat. Sol. (b)* **234** 1 166–71

[5] Schultz A J, Jorgensen J D, Peng J L and Greene R L 1996 *Phys. Rev. B* **53** 5157–59

[6] Richard P, Riou G, Hetel I, Jandl S, Poirier M and Fournier P 2004 *Phys. Rev. B* **70** 064513

[7] Matsuura M, Dai P, Kang H J, Lynn J W, Argyriou D N, Prokes K, Onose Y and Tokura Y 2003 *Phys. Rev. B* **68** 144503

[8] Riou G, Richard P, Jandl S, Poirier M, Fournier P, Nekvasil V, Barilo S N and Kurnevich L A 2004 *Phys. Rev. B* **69** 024511

[9] Higgins J S, Dagan Y, Barr M C, Weaver B D and Greene R L 2006 *Phys. Rev. B* **73** 104510

[10] Gauthier J, Gagné S, Renaud J, Gosselin M-È, Fournier P and Richard P 2007 *Phys. Rev. B* **75** 024424

[11] Kang H J, Dai P, Campbell B J, Chupas P J, Rosenkranz S, Lee P L, Huang Q, Li S, Komiya S and Ando Y 2007 *Nat. Mater.* **6**(3) 224–29

[12] Armitage N P, Fournier P and Greene R L 2010 *Rev. Mod. Phys.* **82** 2421–87

[13] Roberge G, Charpentier S, Godin-Proulx S, Rauwel P, Truong K D and Fournier P 2009 *J. Cryst. Growth* **311** 1340–45

[14] Kurahashi K, Matsushita H, Fujita M and Yamada K 2002 *J. Phys. Soc. Jpn.* **71**(3) 910–5

[15] Mang P K, Larochelle S, Mehta A, Vajk O P, Erickson A S, Lu L, Buyers W J L, Marshall A F, Prokes K and Greven M 2004 *Phys. Rev. B* **70** 094507

[16] Kimura H, Noda Y, Sato F, Tsuda K, Kurahashi K, Uefuji T, Fujita M and Yamada K 2005 *J. Phys. Soc. Japan* **74** 8 2282–86

[17] Prasad Beesabathina D, Salamanca-Riba L, Mao S N, Xi X X and Venkatesan T 1993 *Appl. Phys. Lett.* **62** 23 3022–4

[18] Mao S N, Xi X X, Qi Li, Venkatesan T, Prasad Beesabathina D, Salamanca-Riba L, Wu X D 1994 *J. Appl. Phys.* **75** 4 2119–24

[19] Naito M, Karimoto S and Tsukada A 2002 *Supercond. Sci. Technol.* **15**(12) 1663.

[20] Guarino A, Fittipaldi R, Romano A, Vecchione A and Nigro A 2012 *Thin Solid Films* **524**(0) 282–9

[21] Williams D B and Carter C B 2009 *Transmission Electron Microscopy: A Textbook for Material Science* (New York: Springer Science+Business Media) p 393

[22] Kubo S and Suzuki M 1991 *Physica C* **185-189** 1251-2

[23] Jiang W, Mao S N, Xi X X, Jiang X, Peng J L, Venkatesan T, Lobb C J and Greene R L 1994 *Phys. Rev. Lett.* **73** 1291–4

[24] Charpentier S, Roberge G, Godin-Proulx S, Béchamp-Laganière X, Truong K D, Fournier P and Rauwel P 2010 *Phys. Rev. B* **81** 104509

[25] Xu X Q, Mao S N, Jiang W, Peng J L and Greene R L 1996 *Phys. Rev. B* **53** 871–5

[26] Vaglio R, Attanasio C, Maritato L and Ruosi A 1993 *Phys. Rev. B* **47** 22 15302–3

[27] Song D, Park S R, Kim C, Kim Y, Leem C, Choi S, Jung W, Koh Y, Han G, Yoshida Y, Eisaki H, Lu D H, Shen Z X and Kim C 2012 *Phys. Rev. B* **86** 144520

[28] Gupta A, Koren G, Tsuei C C, Segmüller A and McGuire T R 1989 *Appl. Phys. Lett.* **55**(17) 1795–7

[29] Brinkmann M, Rex T, Stief M, Bach H and Westerholt K 1996 *Physica C* **269**(12) 76 – 82

[30] Mao S N, Jiang W, Xi X X, Li Q, Peng J L, Greene R L, Venkatesan T, Beesabathina D P, Salamanca-Riba L and Wu X D 1995 *Appl. Phys. Lett.* **66**(16) 2137–9